

Evaluation of Osteoconductive Scaffolds in the Canine Femoral Multi-Defect Model

Viviane Luangphakdy, MS,¹ Esteban Walker, PhD,² Kentaro Shinohara, MD, PhD,¹
Hui Pan, MD, PhD,¹ Theresa Hefferan, PhD,³ Thomas W. Bauer, MD, PhD,⁴ Linda Stockdale, MAT,⁵
Sunil Saini, PhD,⁶ Mahrokh Dadsetan, PhD,³ M. Brett Runge, PhD,³ Amit Vasniji, PhD,⁷
Linda Griffith, PhD,⁵ Michael Yaszemski, MD, PhD,³ and George F. Muschler, MD^{1,8}

Treatment of large segmental bone defects remains an unsolved clinical challenge, despite a wide array of existing bone graft materials. This project was designed to rapidly assess and compare promising biodegradable osteoconductive scaffolds for use in the systematic development of new bone regeneration methodologies that combine scaffolds, sources of osteogenic cells, and bioactive scaffold modifications. Promising biomaterials and scaffold fabrication methods were identified in laboratories at Rutgers, MIT, Integra Life Sciences, and Mayo Clinic. Scaffolds were fabricated from various materials, including poly(L-lactide-co-glycolide) (PLGA), poly(L-lactide-co- ϵ -caprolactone) (PLCL), tyrosine-derived polycarbonate (TyrPC), and poly(propylene fumarate) (PPF). Highly porous three-dimensional (3D) scaffolds were fabricated by 3D printing, laser stereolithography, or solvent casting followed by porogen leaching. The canine femoral multi-defect model was used to systematically compare scaffold performance and enable selection of the most promising substrate(s) on which to add cell sourcing options and bioactive surface modifications. Mineralized cancellous allograft (MCA) was used to provide a comparative reference to the current clinical standard for osteoconductive scaffolds. Percent bone volume within the defect was assessed 4 weeks after implantation using both MicroCT and limited histomorphometry. Bone formed at the periphery of all scaffolds with varying levels of radial ingrowth. MCA produced a rapid and advanced stage of bone formation and remodeling throughout the defect in 4 weeks, greatly exceeding the performance of all polymer scaffolds. Two scaffold constructs, TyrPC_{PL}/TCP and PPF_{4SLA}/HA_{PLGA} Dip₇, proved to be significantly better than alternative PLGA and PLCL scaffolds, justifying further development. MCA remains the current standard for osteoconductive scaffolds.

Introduction

THIS PROJECT WAS designed to rapidly assess and compare promising biodegradable osteoconductive scaffold compositions without bioactive molecules for the treatment of critical size bone defects. This study describes the first step in a systematic effort to develop new bone regeneration methods for treatment of large segmental bone defects that combine scaffolds, sources of osteogenic cells, and bioactive scaffold modifications.

In both the military and civilian population, treatment of large segmental bone defects remains an unsolved clinical challenge, despite a wide array of existing bone graft mate-

rials. Extremity injuries represent 58%–88% of all traumatic injuries in United States armed conflicts.¹ These fractures are frequently comminuted, complicated by extensive soft-tissue loss, and have segmental bone defects ranging from 0 to 20 cm. The biological challenge of bone regeneration is made more complex by associated regional soft tissue loss, reduced local vascularity, and regional scarring that follow both the initial injury and any secondary infections that occur. Bone defects are most frequent in the tibia; however, defects in the femur, humerus, radius, ulna, and mandible are also common. Clinical success in regenerating bone in these defects can be achieved using one or more of several current methods and materials. However, success is variable, even in the

Departments of ¹Biomedical Engineering and ²Quantitative Health Sciences, Cleveland Clinic, Cleveland, Ohio.

³Departments of Orthopedic Surgery and Biomedical Engineering, Mayo Clinic College of Medicine, Rochester, Minnesota.

⁴Departments of Pathology, Cleveland Clinic, Cleveland, Ohio.

⁵Department of Biological Engineering, Massachusetts Institute of Technology, Cambridge, Massachusetts.

⁶Integra Life Sciences, Plainsboro, New Jersey.

⁷ImageIQ, Inc., Cleveland, Ohio.

⁸Department of Orthopaedic Surgery, Cleveland Clinic, Cleveland, Ohio.

hands of highly skilled and experienced surgeons. Moreover, even when success is achieved, the time necessary to achieve it is often prolonged and characterized by multiple procedures and complications.

Effective bone tissue engineering in the setting of a segmental bone defect requires both an awareness and rational management of multiple factors. These include the use of osteoconductive scaffolds, osteogenic cells, osteoinductive and osteopromotive stimuli, and the provision of both an appropriate biomechanical environment and mass transport environment. Each of the critical variables contributes, in combination with the others, to success or failure.² Osteoconductive scaffolds, the focus of this work, may serve multiple functions, providing (1) a space holder that prevents encroachment of surrounding tissues into the graft site; (2) a three-dimensional (3D) lattice or surface that facilitates the attachment, survival, migration, proliferation, and differentiation of stem cells and progenitor cells promoting the distribution of a bone healing response throughout the grafted volume; (3) a vehicle for delivery of cells into a graft site, facilitating their retention and distribution throughout the region where new tissue is desired; and/or (4) a vehicle for presentation or delivery of bioactive agents.³⁻⁶

Autogenous cancellous bone (ACB) frequently harvested from the iliac crest is currently considered to be the most effective bone graft material for bone defects. ACB provides a degradable osteoconductive scaffold in the form of mineralized trabecular bone that will undergo osteoclast-mediated remodeling and replacement with native bone. This remodeling may also release bioactive factors that provide osteoinductive and osteopromotive stimuli in the bone defect site. In addition, ACB includes the transplantation of a population of osteogenic cells that are resident on the trabecular surface and in the marrow space. However, the availability of autograft material is limited, and often insufficient for large defects. Moreover, the harvesting of ACB is associated with blood loss, pain, scarring, and the potential for infection and secondary disability.

Human bone allograft, processed from cadaveric donors, has been the preferred osteoconductive matrix when sufficient ACB is either unavailable or is contraindicated due to associated morbidity. Allograft is available in any volume that is needed. It is also available in many formulations (blocks, chips, fibers, powders) that can be customized for specific clinical settings. However, by far, the most common formulation of allograft for bone grafting procedures is mineralized cancellous allograft (MCA) (commonly referred to as "chips" or "croutons").

A broad range of alternative scaffolds is already available for clinical use, and many new scaffolds are under development. Differences between scaffolds can be generally categorized into six domains: bulk material, 3D architecture and porosity, surface chemistry, mechanical properties, initial scaffold environment (osmolarity, pH), and late scaffold environment (degradation characteristics). Each domain has important implications for both the biological response of local tissues to a scaffold and for a given scaffold's utility in transplanting or supporting local stem cells and progenitors.²

Clinically available scaffolds are made from a broad range of bulk materials. These include tissue-derived materials (e.g., allograft bone matrix, skin, intestinal submucosa), biological polymers (e.g., collagen, hyaluronan, fibrin, alginate),

ceramics or mineral-based matrices (e.g., tricalcium phosphate, hydroxyapatite, calcium sulfate), metals (e.g., titanium, tantalum, and other alloys), or composites of two or more materials.^{2,7,8} A variety of synthetic water-insoluble polymers are also being adapted or developed. These include, but are not limited to, poly(lactide), tyrosine-derived polycarbonates (TyrPCs),⁹⁻¹² poly(caprolactone), poly(propylene fumarate) (PPF),¹³⁻¹⁵ and synthetic hydrogels [e.g., poly(ethylene oxide)based materials].¹⁶⁻¹⁸ The potential advantage of these alternative synthetic scaffolds over allograft is an increase in reproducibility, a reduction in production cost, the potential for custom fabrication to fit the shape of defined defects, and the capacity to be used as a substrate material. The substrate material can then undergo systematic improvement through changes in its architecture, surface chemistry, mechanical and degradation properties, and local delivery of drugs or bioactive agents.

The work described in this report was designed to (1) rapidly assess and compare several promising osteoconductive biodegradable scaffolds, (2) compare their performance to the current standard for osteoconductive materials (MCA), and (3) in doing so, identify one or more scaffold constructs worthy of further optimization as delivery vehicles for use in combination with sources of osteogenic cells and/or presentation or delivery of bioactive agents.

Materials and Methods

Implant materials

Four biomaterials laboratories were recruited into the Limb Salvage Program in the Rutgers-Cleveland Clinic Consortium of the Armed Forces Institute for Regenerative Medicine (AFIRM). The overall aim of the AFIRM limb salvage program is the rapid development of new therapeutic strategies that specifically target the needs of wounded warriors and victims of civilian trauma who face the challenge of large segmental bone defects. The strategy proposed here was to systematically and competitively assess each laboratory's best available degradable synthetic biomaterial scaffolds for bone regeneration, comparing their performance to each other and against current clinical standards. In doing so, one or more scaffold substrates would be selected for further development as a carrier (a delivery system) for osteogenic cells and bioactive agents. Participating laboratories and investigators included The New Jersey Center for Biomaterials at Rutgers University (Lab Director Joachim Kohn, PhD), the Mayo Clinic Tissue Engineering and Polymeric Biomaterials Laboratory (Lab Director Michael Yaszemski, MD, PhD), the Griffith Lab Massachusetts Institute of Technology (Lab Director Linda Griffith, PhD), and Therics, LLC (formerly of the Theken family of companies, Akron, OH). Therics and MIT provided both materials for evaluation, and also made the fabrication strategy of three-dimensional printing (3DP) available to other collaborators.¹⁸⁻²¹ Each laboratory had a history of biomaterials with efficacy in small animals.^{9-12,14,22-28}

The tested scaffolds are outlined in Table 1, which provides a brief summary of the bulk material, fabrication process, pore geometry, use of calcium containing components, and method of sterilization used in each case.

The bulk polymer materials that were evaluated included 70:30 Poly(L-lactide-co- ϵ -caprolactone) (PLCL; Boehringer

TABLE 1. SUMMARY OF IMPLANTED SCAFFOLD MATERIALS

Exp.	Scaffold	Fabrication	Macropore size	Micropore size	Well thickness	% void	Molecular weight	Calcium-containing components	Sterilization
1	PLGA/TCP _{3DP}	3DP	~50–150 μm	None	500 μm	70–80	144 k	β-TCP:scaffold 70:30 wt:wt	EtO then 24 h degasing
	PLCL/TCP _{3DP}	3DP	~50–150 μm	None	500 μm	70–80	96 k	β-TCP:scaffold 70:30 wt:wt	EtO then 24 h degasing
2	TyrPC/TCP _{3DP}	3DP	~50–150 μm	None	500 μm	70–80	218 k	β-TCP:scaffold 50:50 wt:wt	EtO then 24 h degasing
3	TyrPC _{3DP}	3DP	~50–150 μm	None	500 μm	70–80	210 k	None	EtO then 24 h degasing
	TyrPC _{3DP}	3DP	~50–150 μm	None	500 μm	70–80	210 k	None	EtO then 24 h degasing
	TyrPC _{PL}	PL	~212–425 μm	~10–50 μm	~1–100 μm	85–95	200 k	None	EtO then 24 h degasing
4	PPF _{2SLA} /HA _{PLGA} DP	SLA	1000 μm	None	500 μm	80	2 k ^a	Dip coat w/ HA/PLGA in chloroform	70%EtOH 30 min then UV irradiation for 1 h
	PPF _{4SLA} /HA _{PLGA} DP	SLA	1000 μm	None	500 μm	80	4 k ^a	Dip coat w/ HA/PLGA in chloroform	70% EtOH 30 min then UV irradiation for 1 h
5	PLCL/TCP _{3DP}	3DP	~50–150 μm	None	500 μm	70–80	96 k	β-TCP:scaffold 70:30 wt:wt	EtO then 24 h degasing
	PLCL/TCP _{3DP} + BMC	3DP	~50–150 μm	None	500 μm	70–80	96 k	β-TCP:scaffold 70:30 wt:wt	EtO then 24 h degasing
6	PPF _{2SLA} /HA _{PLGA} Spray	SLA	1000 μm	None	500 μm	80	2 k ^a	Spray coat w/ HA/PLGA in chloroform	70% EtOH 30 min then UV irradiation for 1 h
	PPF _{2SLA} /TCP _{PLGA} Spray	SLA	1000 μm	None	500 μm	80	2 k ^a	Spray coat w/ TCP/PLGA in chloroform	70% EtOH 30 min then UV irradiation for 1 h
7	TyrPC _{PL} /TCP	PL	~212–425 μm	~10–50 μm	~1–100 μm	85–95	200 k	50:50 wt:wt scaffold: TCP ratio	EtO then 24 h degasing
	TyrPC _{PL} /CaCl ₂	PL	~212–425 μm	~10–50 μm	~1–100 μm	85–95	200 k	40:60 wt:wt scaffold:CaCl ₂ ratio	EtO then 24 h degasing
8	MCA	CM	N/A	N/A	N/A	N/A	N/A	Native Mineral	Sterile harvest and processing
	MCA + BMC	CM	N/A	N/A	N/A	N/A	N/A	Native Mineral	Sterile harvest and processing

^aMolecular weight before formation of a cross-linked network; after cross-linking, molecular weight is essentially infinite.

TyrPC scaffolds and characterization was provided by Joachim Kohn, New Jersey Center for Biomaterials, Rutgers University.

PLCL, poly(L-lactide-co-ε-caprolactone); PLGA, poly(L-lactide-co-glycolide); PPF, poly(propylene fumarate); β-TCP, β tri-calcium phosphate; CaCl₂, calcium chloride; SLA, stereolithography; PL, porogen leaching method; 3DP, three-dimensional printing; CM, clinical methods for human allograft preparation; EtO, ethylene oxide sterilization; BMC, bone marrow clot; TyrPC, tyrosine-derived polycarbonate; MCA, mineralized cancellous allograft; N/A, not applicable.

Ingelheim, Petersburg, VA); 82:18 Poly(L-lactide-co-glycolide) (PLGA; Boehringer Ingelheim)²⁹; Tyrosine-derived polycarbonate (Kohn Laboratory, Rutgers University); and PPF (Yaszemski Lab, Mayo Clinic).^{30–33} Supplementary data describing more details on the PPF material synthesis and fabrication is available online at www.liebertpub.com/tea. All scaffolds were manufactured using previously defined methods into cylinders with dimensions of 0.99 cm diameter and 1.5 cm height. The methods used previously published procedures for fabrication of 3D scaffolds: 3DP,^{28,29,34} stereolithography (SLA),^{13,35} and PL.¹² Figure 1 provides representative images illustrating the variation in structure that was provided using these methods.

Experiments were performed in the order presented. Data from prior experiments were used by each laboratory to guide subsequent modifications of scaffold fabrication and composition. All but three polymeric scaffolds contained a calcium component incorporated into the polymer material. In Experiments 1, 2, and 5, β tri-calcium phosphate (β -TCP) granules with size range of 45–106 μm and a porosity of 65% were used (Therics, LLC, Akron, OH). In Experiments 4 and 6, nanocrystals of hydroxyapatite with an average size of 100 nm (range=20–550 nm) (nanohydroxyapatite; Berkeley Advanced Biomaterials, Berkeley, CA) and β -TCP coatings were applied on PPF scaffolds. In Experiment 7, porogen leached scaffolds with a porosity of ~85%–95% were used. Calcium chloride (Sigma Aldrich, St. Louis, MO) was added through saturation of scaffolds with a 10% calcium chloride solution, or β -TCP granules with a size range of 45–106 μm

(Therics, LLC) were included during the porogen leaching (PL) fabrication process.

MCA bone matrix (canine) was utilized as the reference standard for current clinical practice. MCA was prepared and packaged by the Musculoskeletal Transplant Foundation (MTF; Edison, NJ) using canine bones from the proximal humerus, proximal tibia, and contralateral proximal femur. Donor bone was sterilely harvested from canine subjects used in prior experiments following euthanasia. Harvest, shipping at Cleveland Clinic, and processing at MTF were performed using standardized methods that are in common use for preparation of commercially available mineralized cancellous bone matrix consistent with clinical guidelines established by the American Association of Tissue Banks. Cuboidal chips were prepared with a dimension of roughly 3×3×3 mm to enable uniform packing of 20–25 chips to fill each femoral defect site. Sterile processing was maintained throughout with standard confirmatory cultures. No terminal sterilization was used.

Animals

This study was conducted with approval from the Cleveland Clinic Institutional Animal Care and Use Committee (IACUC), and the Animal Care and Use Review Office (ACURO) of U.S. Army Medical Research and Materiel Command (MRMC). Study animals were cared for in accordance with the principles of the *Guide for the Care and Use of Laboratory Animals*.³⁶

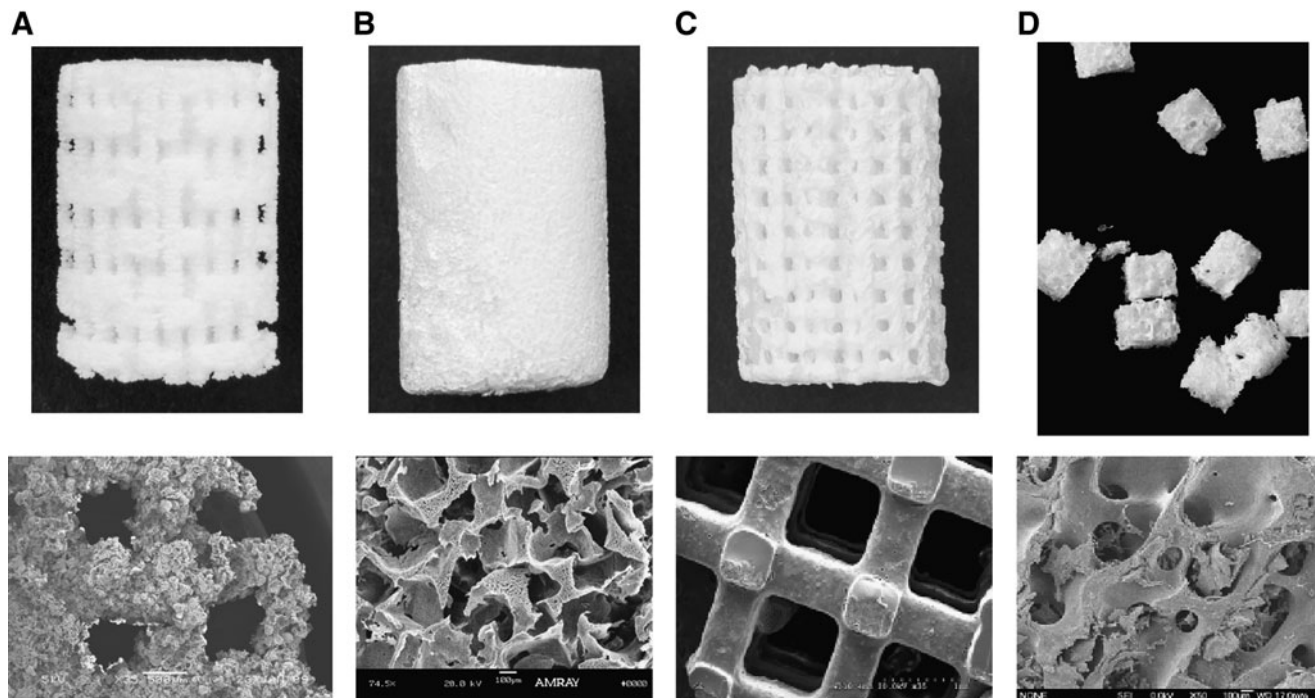


FIG. 1. Implanted scaffolds: (A) PLCL/TCP_{3DP}, (B) TyrPC_{PL}, (C) PPF_{2SLA}, and (D) MCA chips (~3×3 mm). Horizontal scale on lower images is ~4 mm. (SEM image of the TyrPC_{PL} scaffold was provided by Joachim Kohn, New Jersey Center for Biomaterials, Rutgers University.) 3DP, three-dimensional printing; MCA, mineralized cancellous allograft; PL, porogen leaching; PLCL, poly(L-lactide-co-ε-caprolactone); PPF, poly(propylene fumarate); SLA, stereolithography; TCP, tri-calcium phosphate; TyrPC, tyrosine-derived polycarbonate.

Eighty-five adult purposely bred female and male coonhounds (34.3 ± 4.2 kg, age 2.5 years ± 01 months [range 1–5 years]) were used.

Canine femoral multi-defect model

The canine femoral multi-defect (CFMD) model^{37,38} was used for these studies. The CFMD model provides four 10-mm-diameter and 15-mm-long defects for assessment in each subject. These defects are placed in the lateral cortex of the proximal femur. Each defect site is separated by a minimum of 1.5 cm of normal bone and marrow, so that the sites do not interact. The availability of data from four sites in each subject enables comparison of two to four materials while controlling for variation between subjects. The defects are designed to be of sufficient size to create a biological environment in which the interior of the defect is characterized by profound hypoxia, a key feature of large clinical defects that is not modeled in small animal defects. Bone formation and revascularization within the defect occur through a process of ingrowth that has a radially oriented outside-in pattern, which can be readily measured and characterized using microcomputed tomography (MicroCT) and histological methods. As a result, the extent to which a bone healing response progresses into the center of these defects provides an objective comparison of the efficacy of the implanted scaffold materials.

Experimental design

From March 2008 to December 2010, a series of eight experiments were performed between paired materials. The experiments are outlined in Table 1. Each experiment utilized 10 subjects. In each experiment, the two scaffolds (e.g., “A” and “B”) were randomly assigned to either an “ABBA” configuration (five dogs) or a “BAAB” configuration (five dogs) to control for possible site or proximity effects.

Outcome assessment 4 weeks after implantation was selected for two reasons: (1) prior experience using ACB and allograft cancellous bone in this model has demonstrated the potential to achieve robust bone formation and even an advanced state of intramedullary (IM) remodeling in the CFMD model as early as 4 weeks, and (2) those scaffolds that are most effective in initiating rapid onset of bone formation and ingrowth are, we feel, the same scaffolds that are likely to achieve reliable outcomes that represent an advance over existing therapies. Therefore, assessment at later time points might be too late to detect clinically important differences in the rate of onset and extent of new bone formation between scaffolds.

Operative procedure

A fentanyl transdermal patch ($100 \mu\text{g}/\text{h}$) was applied the day before the procedure. Penicillin G (1.2 MillU IM) and atropine (0.02 mg/lb IM) were given on the morning of surgery. General anesthesia was initiated using pentothal (20 mg/kg IV) followed by intubation and closed isoflurane (0.5% – 3%) inhalation. The left hind limb was shaved, prepped, and draped in a sterile fashion. In two cases, Experiments 5 and 8, a single scaffold material was tested with and without bone marrow clot (BMC). In these cases, following the induction of anesthesia, a 2 cc aspirate of bone marrow was harvested from the left proximal humerus using standard clinical technique without an anticoagulant and allowed to clot.^{2,39,40} A 10 cm incision was made on the lateral aspect of the thigh, beginning 4 cm distal to the greater trochanter of the femur. The biceps muscle was then reflected posteriorly and the vastus lateralis was elevated anteriorly in an extra-periosteal plane to expose the anterolateral aspect of the femur. A custom drill guide (Fig. 2) was fixed to the femur using two 3.5-mm-diameter cortical screws (Synthes, Paoli, PA). Four identical 1.0-cm-diameter and 1.5-cm-long cylindrical defects were then created by sequential use of a circular starting trochar, a pointed drill, and a flat finishing drill. A 1.0-cm-diameter by 1.5-cm-long stainless steel spacer was placed in each defect temporarily to allow hemostasis to be achieved without formation of a clot of wound blood in the space that was preserved for the scaffold. The appropriate scaffolds for the particular experiment were then placed in each defect. The graft sites were protected mechanically using a stainless steel plate that was fixed to the femur using two screws placed into the screw holes created for initial fixation of the drill guide. The vastus lateralis was then replaced over the defect sites and under the biceps in an anatomic position. The wound was closed using 0 vicryl sutures to re-approximate the deep fascia, followed by 2-0 vicryl sutures in subcutaneous and subcuticular layers, and then staples in the skin.

Animal care

Animals were allowed free access to food and water and returned to full weight bearing with daily exercise. Agitation in the early postoperative period was managed using acepromazine (0.1 mg/kg SQ). Postoperative pain was managed with the transdermal fentanyl ($100 \mu\text{g}/\text{h}$) patch for 3–6 days, supplemented by Buprenorphine as needed.

Euthanasia was performed 4 weeks after implantation using Beuthanasia™ solution (5 mL/ 5 kg IV; Merck Animal

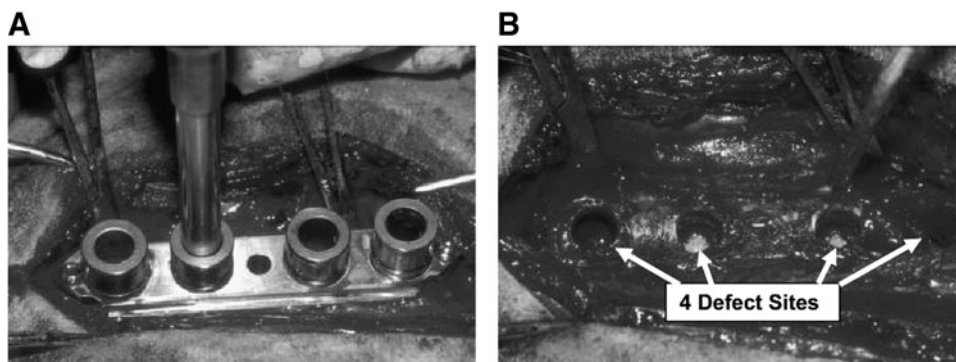


FIG. 2. (A) Drill guide in position on the lateral surface of the proximal femur. (B) Defect sites before implantation of scaffolds.

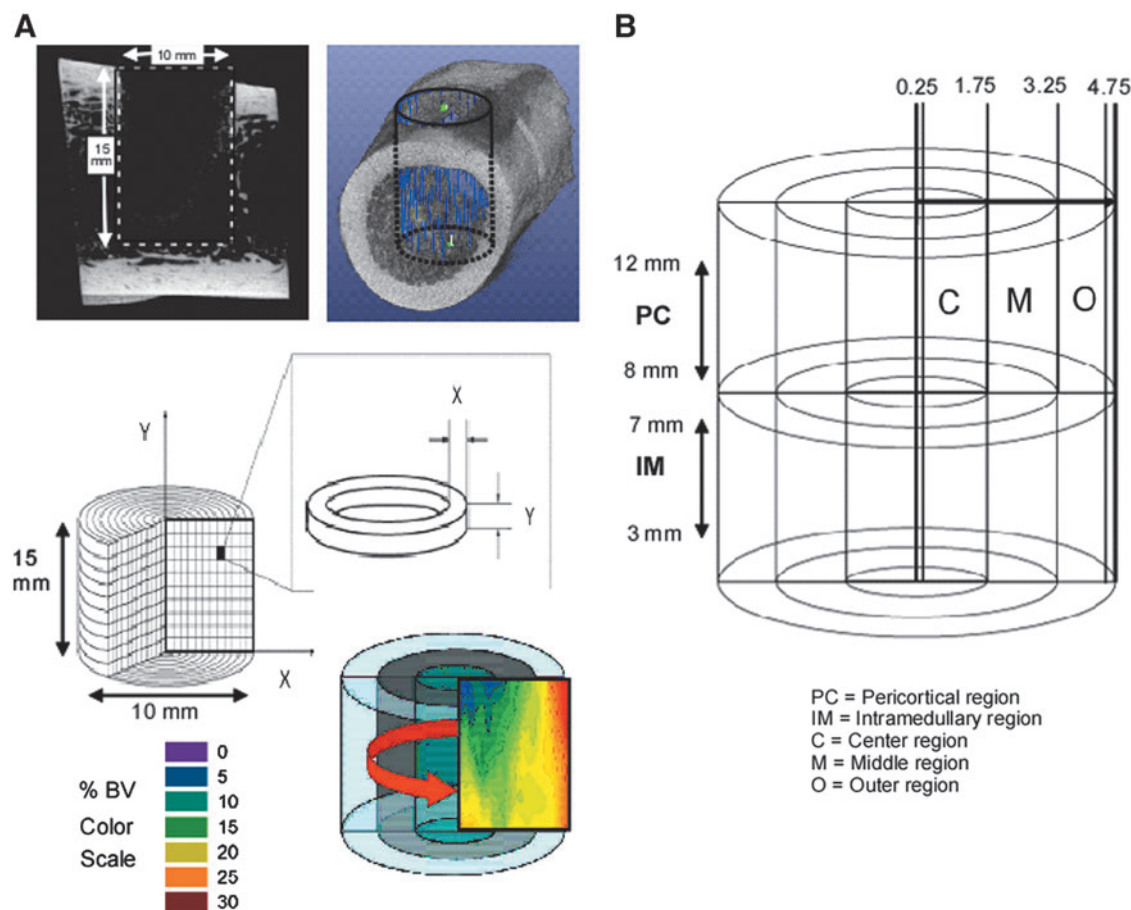


FIG. 3. Micro computed tomography processing technique. **(A)** The 3D defect volume is defined using a standard 10-mm-diameter \times 15-mm-long cylinder. Following segmentation, bone volume (BV) data are mapped onto a color 2D contour plot using a scale from 0% to 30% BV. **(B)** The defect site is divided for analysis into regions for analysis. The pericortical (PC) region and the intramedullary (IM) region are defined based on vertical position from the bottom of the defect. Three regions of depth are defined based on radial distance from the center in millimeters: center (C)=0.25–1.75 mm, middle (M)=1.75–3.25 mm, and outer (O)=3.25–4.75 mm.

Health, Summit, NJ). The plate spanning the defects was removed. The femur was explanted and cleared of adhering tissue. Individual defect sites were separated using a band saw and fixed in 10% neutral buffered formalin. After 48 h, the solution was replaced with 70% ethanol to prevent demineralization. MicroCT images were obtained of each graft site prior to processing for histological assessment.

MicroCT processing and analysis

Quantitative assessment of each graft site was performed using MicroCT and 3D segmental image postprocessing (Fig. 3). Scanning was done with an eXplore Locus MicroCT scanner (GE Healthcare, Milwaukee, WI) at 45 micron resolution, 360 projections acquired every degree of rotation. The system was operated at 80 kV, 500 μ A, with an exposure time of 500 ms per individual projection. A dark-field (X-ray beam turned off), a bright field (X-ray beam turned on with no sample in beam), and density phantom (hydroxyapatite, solid water, air) image was taken at the end of each imaging session for correction of the X-ray projection data (dark- and bright-field normalization, ring artifact reduction, and CT attenuation to Hounsfield Unit conversion during projection reconstruction). Each defect was positioned with the cranial-

caudal axis (i.e., the cross-sectional plane of the cylindrical specimen) parallel to the direction of table travel.

Regions of bone formation within the defect site were identified based on calibrated Hounsfield Units (HU) representing native trabecular bone (1000 ± 100 HU) within each sample to provide reproducible thresholding across all specimens by an operator who was blinded with respect to the material being assessed. A 3D cylindrical defect template, 10 mm in diameter and 15 mm in length size, was manually positioned to define the boundaries of the defect site using the circular introitus and marks from the flat finishing drill on the opposite cortex as fiduciary guides (Fig. 3). Voxels within the defect site above the threshold value for trabecular bone were identified and segmented as new bone. Percent bone volume (% BV) was measured by determining the fraction of bone voxels within the defect site volume. The pattern and density of bone formation in each defect was plotted for visualization by projecting % BV data as a 2D contour plot using a color range of 0%–30% BV. The X-axis indicates radial position from the center of the defect to the edge (range 0–5 mm), and the Y-axis represents vertical position within the defect from the bottom to the opening at the lateral cortex (range 0–15). Data for the 20 samples of each scaffold that were evaluated in each paired experiment were

combined to project the mean % BV for each scaffold. For analysis, the defect sites were subdivided into regions of interest based on differences in local tissue environment. The pericortical (PC) region (between 8 and 12 mm from the bottom of the grafted site) represents the region of the graft site that is adjacent to the cortex, where the contribution of cells from periosteum, cortex, and endosteum may contribute to new bone formation. In contrast, the IM region (between 3 and 7 mm from the bottom of the grafted site) is separated, by several millimeters, from the endosteal source of osteogenic cells and bounded only by cells from the marrow cavity (See Fig. 3). The PC and IM regions are further divided into a center, middle, and outer region based on the radial position within the defect site. The scaffold performance in the center-most region of the defect was considered to be the most discriminating with respect to likely efficacy in larger defects, and therefore serves as the primary outcome parameter for comparison between scaffolds.

To minimize the confounding effects of variation in % BV unrelated to scaffold performance, the region of interest for analysis of data within the defect sites was carefully defined. Variation due to nonradially oriented boundary effects at the top soft tissue interface and the bottom trabecular bone interface was minimized by eliminating the top and bottom 3 mm of each defect from analysis. The axial center (radius = 0–0.25 mm) was removed from analysis due to the vanishingly small sampling volume that is assessed as one approaches a radius of zero. This creates high variability in data near the axial center. Finally, data from the very edge of each defect (radius = 4.75–5.0 mm) were also removed to minimize the probability of random inclusion of existing cortex in the analysis of the PC region resulting from the positioning of the defect template.

Histology analysis

Histology was used as a secondary qualitative outcome parameter and primarily as a means of (1) screening for evidence of local inflammation that might be induced by a particular implant, (2) provisional assessment of the rate of bulk degradation taking place for a given scaffold (both bulk polymer and any remaining calcium containing component), (3) validation of the % BV data obtained using MicroCT, and (4) screening for important differences in the nature and quality of bone and soft tissue remodeling between different scaffolds. Two defect sites for each material were assessed by histomorphometry in each experiment, representing a subsampling of 10% for each material. All samples were processed and analyzed in the Bone Histomorphometry Laboratory at the Mayo Clinic using undecalcified processing. Each specimen was dehydrated, embedded in methacrylate, and polymerized. Sections with 5- μ m thickness were cut using a Leica RM 2265 microtome and stained using both Goldner's Trichrome, and hematoxylin and eosin (H&E). The Goldner's trichrome-stained sections were scanned using a NanoZoomer Digital Pathology System (Hamamatsu, Bridgewater, NJ) and analyzed using the software package IHC score (Bacus Labs, Lombard, IL) to measure the percent of bone volume, the percent of nonbone cellular matrix, the percent of residual implant, and nontissue or implant spaces or artifacts. Because the IHC score does not distinguish between remaining unresorbed allograft and newly formed bone tissue, additional manual analysis was performed on samples of containing

MCA scaffold using the OsteoMeasure system (OsteoMetrics, Decatur, GA) to estimate the relative contribution of new bone versus residual allograft to the total bone measurement provided by MicroCT. In order to provide systematic and representative sampling, a contiguous series of 20 \times magnification fields were examined extending in a transaxial plane across the defect site through the mid-portion of the PC region. Regions of cellular new bone and acellular residual allograft were traced. Total bone area was expressed as a percentage of the tissue area measured. The relative area of new bone and residual allograft was expressed as a percentage of the total bone area. Scaffolds containing TCP and HA when implanted were also examined to look for evidence of residual TCP or HA that could add mineral density and result in an artifactual increase the overall % BV estimates.

Statistical analysis

Statistical analysis was performed on individual experiments as they were completed. The mean % BV in the center, middle, and outer depths of the PC and IM regions of each defect was used as response variables. Due to extreme skewness (Fig. 4), the data were transformed using the log function. The analyses were performed using a mixed effect analysis of variance (ANOVA) that included scaffold, position, region, and distance to the center. Interactions were tested. Dog was included as a random effect.

The analysis of the combined data from the eight experiments was performed using SAS[®] software (SAS[®], Cary, NC) and JMP[®] 9.0.0 software (SAS[®]). The analysis was done with a similar mixed effect ANOVA model. The Tukey-Kramer method for multiple paired comparisons was used to separate the means for the scaffolds. The significance level was set at $p=0.05$.

Results

Animal care

Nine of the 85 canine subjects (10%) developed a fracture of the femur resulting in immediate euthanasia and exclusion from further analysis. There were no other complications.

MicroCT % BV data

Two-dimensional contour plots of % BV are presented in Figure 5, illustrating the pattern, distribution, and density of bone formation for all scaffolds. As in prior assessments using the CFMD, the highest percent bone volume was found nearest the periphery of the defect, with variable levels of penetration into the middle and central regions. In addition, in all cases, % BV was highest in the PC region of the defect, and lower in the IM region. These images also illustrate that the bone formation realized after implantation of MCA far exceeded that of all other scaffold constructs.

In Figure 6, the % BV data for all scaffold materials are presented as 2D plots that illustrate the quantitative change in % BV relative to depth within the defect. Data for the overall defect, the PC region alone, and the IM region alone are presented separately. These plots illustrate that marked differences in % BV were seen between scaffolds in the outer, middle, and center region of the defect site. Bone formation was greatest at the periphery of the defect (outer region) and decreased as one progressed to the middle and center regions

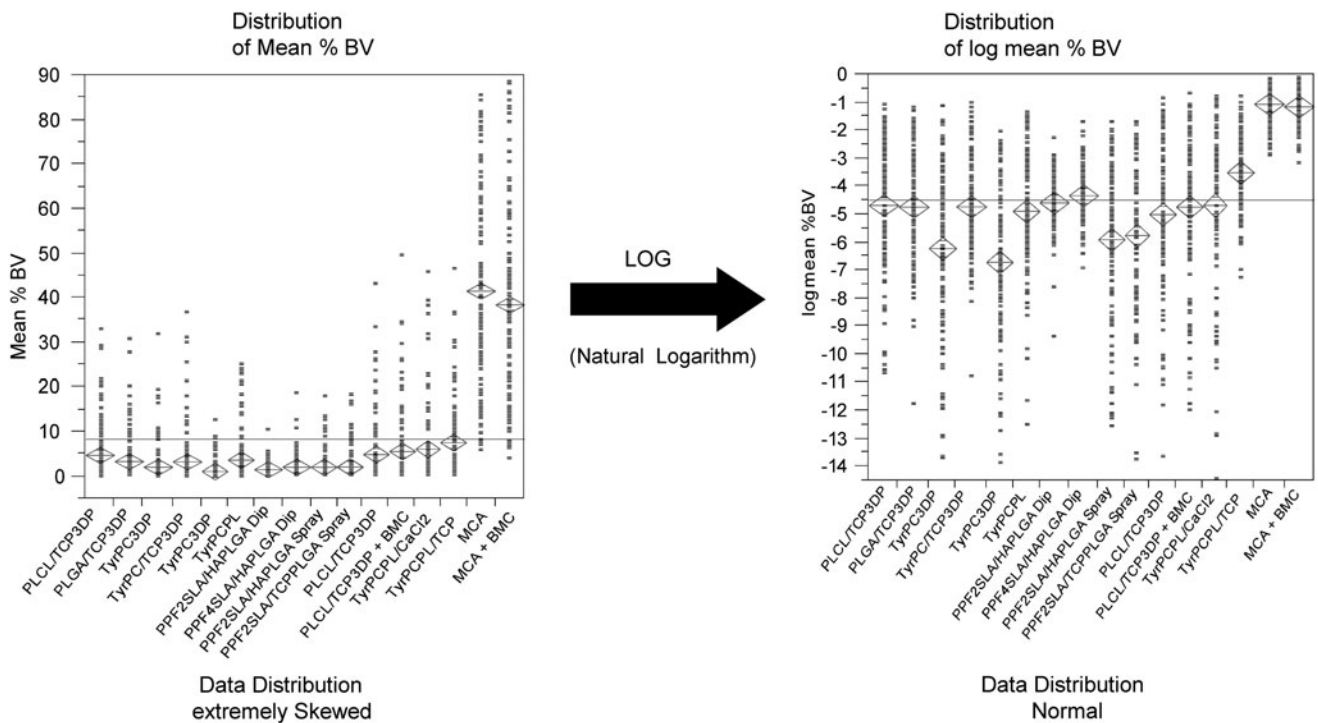


FIG. 4. Percent bone volume (% BV) raw data distribution for the overall defect site is extremely skewed toward low values for all scaffolds except MCA. This was adjusted to enable parametric analysis by applying the logarithm transformation.

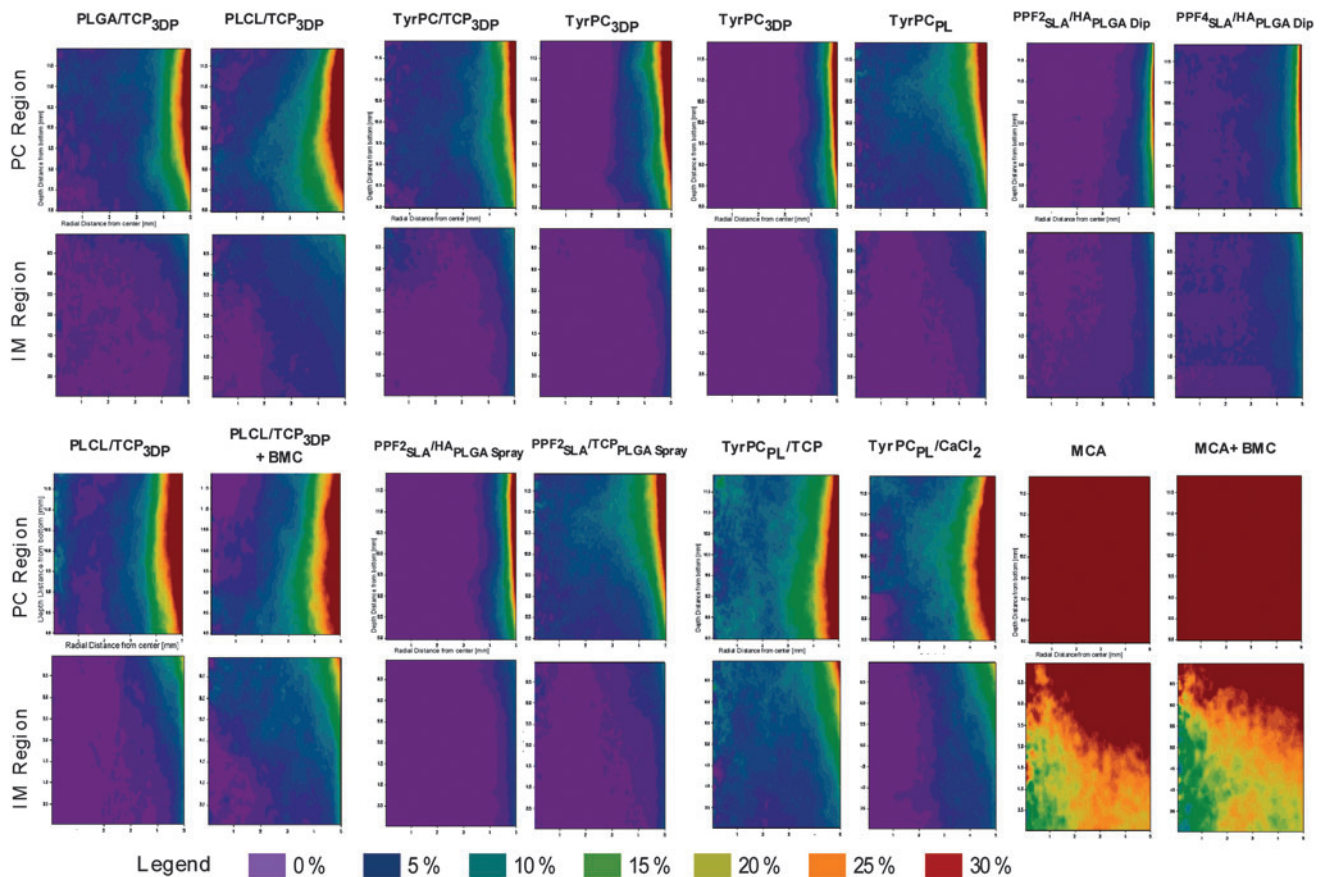


FIG. 5. Two-dimensional contour plots of bone volume percent using color map ranging from 0% (purple) to 30% (red).

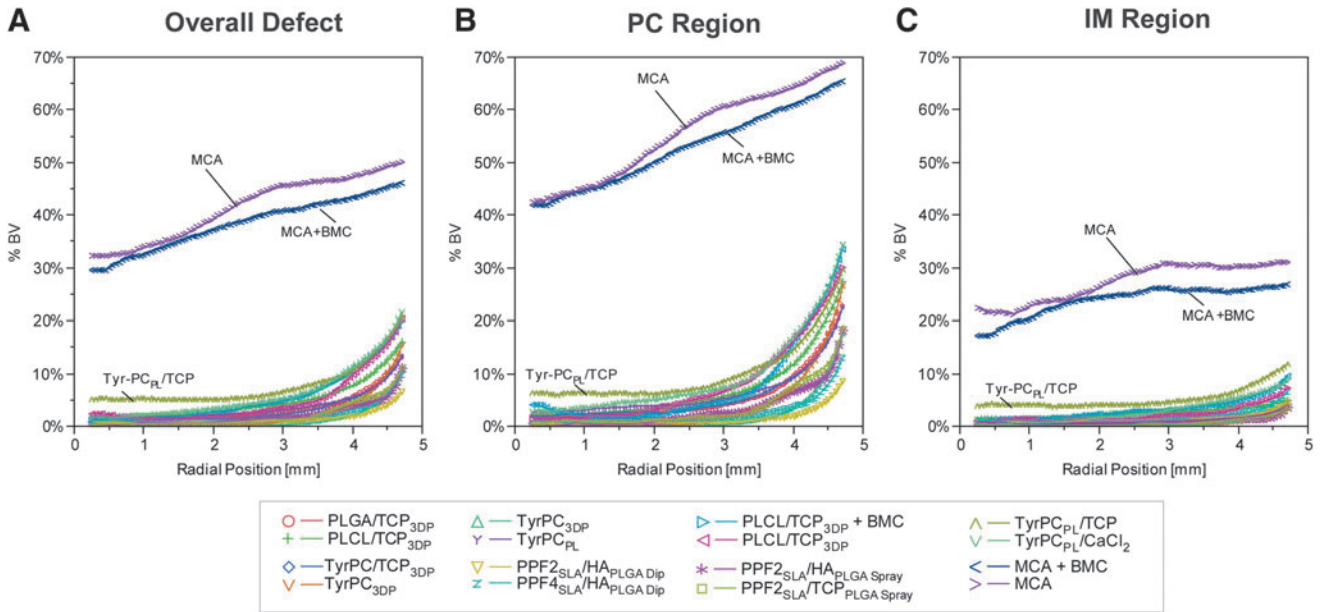


FIG. 6. Percent bone volume (% BV) plotted versus radial position for (A) the entire defect volume, (B) the PC region, and (C) the IM region. BMC, bone marrow clot.

in all scaffolds. % BV was consistently two- to threefold greater in the PC region than in the IM region at each region of depth.

The MCA scaffold resulted in a four- to sixfold greater % BV than any of the polymer scaffolds. When MCA was used, the arithmetic mean % BV in the PC region was 40% or greater all the way to the center of the defect. In the most clinically relevant center area (radial position 0.25–1.75 mm), the mean % BV for one polymer scaffold, TyrPC_{PL}/TCP tended to rise above the other scaffolds, approaching an arithmetic mean of 5%.

The histogram shown in Figure 6 plots the distribution of % BV data for all implants using each material, and the effect of the log transformation that was performed to improve normality. Table 2 presents the result of the Tukey-Kramer analysis that compared scaffolds based on % BV in the overall defect region (radial range 0.25–4.75 mm and depth range 3–

12 mm). Performance differed significantly from one scaffold to another ($p < 0.0001$). Table 3 presents the result of the Tukey-Kramer analysis that compared scaffolds in the most biologically challenging center (radial position 0.25–1.75 mm) of the IM region. MCA displayed significantly higher % BV than any polymer scaffold tested ($p < 0.0001$) in both analyses.

The geometric mean % BV for MCA was 34.6% in the overall defect region and 19.5% in the center IM region. The geometric mean % BV for the best performing polymer scaffold, TyrPC_{PL}/TCP, was 3.00% in the overall defect region and 1.11% in the center IM region. The geometric mean % BV for the next highest performing polymer scaffold, PPF4_{SLA}/HA_{PLGA} Dip, was 1.32% and 0.96% in the overall defect and center IM regions, respectively.

The TyrPC_{PL}/TCP and PPF4_{SLA}/HA_{PLGA} Dip scaffolds were statistically superior to all other polymer scaffolds when

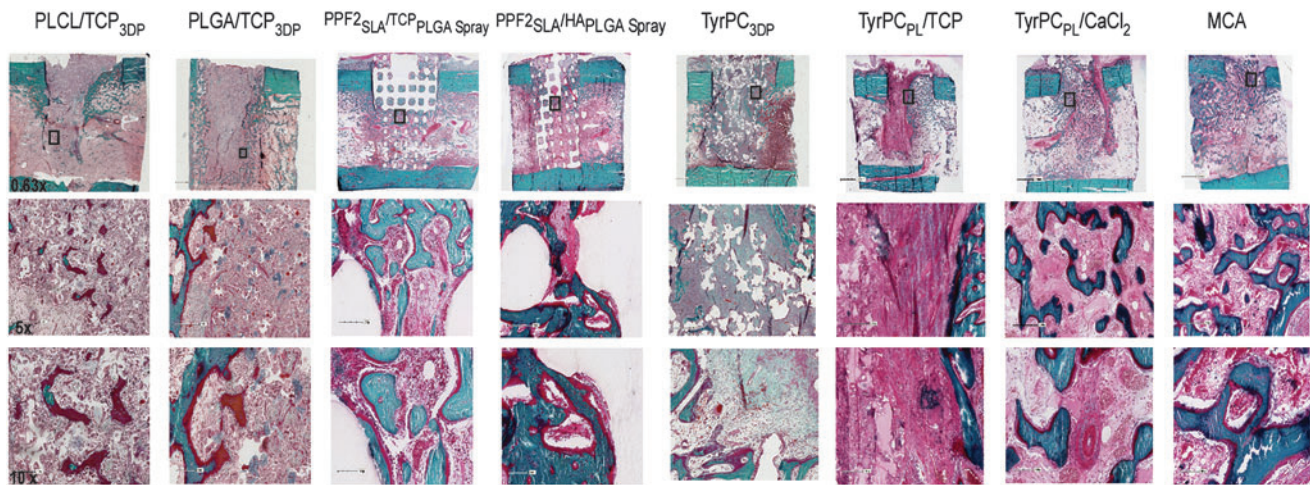


FIG. 7. Undecalcified histology: Representative images for selected scaffold constructs stained using Goldner's Trichrome. Magnification at 1×, 5×, 10×. The black square box indicates the region of defect where the 5× magnification is presented.

TABLE 2. GROUP SEPARATION TABLE OBTAINED BY TUKEY-KRAMER METHOD ANALYSIS IN THE OVERALL DEFECT REGION

	Groups ^a			Mean (log)	Geometric mean (% BV)
MCA	A			-1.06	34.64
MCA + BMC	A			-1.15	31.65
TyrPC _{PL} /TCP		B		-3.51	3.00
PPF4 _{SLA} /HA _{PLGA} Dip		B	C	-4.33	1.32
PPF2 _{SLA} /HA _{PLGA} Dip			C	-4.59	1.02
TyrPC _{PL} /CaCl ₂			C	-4.68	0.93
PLCL/TCP _{3DP}			C	-4.68	0.93
TyrPC/TCP _{3DP}			C	-4.73	0.88
PLGA/TCP _{3DP}			C	-4.73	0.88
PLCL/TCP _{3DP} + BMC			C	-4.74	0.88
TyrPC _{PL}			C	-4.89	0.75
PLCL/TCP _{3DP}			C	-5.00	0.67
PPF2 _{SLA} /TCP _{PLGA} Spray			D	-5.76	0.32
PPF2 _{SLA} /HA _{PLGA} Spray			D	-5.91	0.27
TyrPC _{3DP}			D	-6.22	0.20
TyrPC _{3DP}			D	-6.71	0.12

^aScaffold formulations that are designated by the same letter group are statistically not different from each other, but are statistically different from scaffolds in nonoverlapping groups. The formulations labeled "A" had greater % bone volume than all other scaffolds.

compared based on % BV in the overall defect region (both scaffolds are in Group B in Table 2) and in the center IM region (both scaffolds are not in Group D in Table 3). However, TyrPC_{PL}/TCP and PPF4_{SLA}/HA_{PLGA} Dip scaffolds were not statistically different from each other with respect to % BV (both are always in the same group in Tables 2 and 3).

In the two settings where the MCA and PLCL/TCP_{3DP} scaffolds were tested with and without a BMC, there was no evidence that the addition of BMC changed the biological performance of the scaffold with respect to % BV.

Histology

Representative histology images are provided for each scaffold material in Figures 7–9. New tissue formation occurred with little evidence of inflammation and no evidence of infection.

Defects grafted with MCA were found to have bridging bone across the PC region. Active osteoclastic resorption of residual allograft was seen throughout the samples, with bone formation on all allograft surfaces. Unmineralized osteoid was thicker and covered more bone surface in the PC region, suggesting more active bone formation in the PC region than in the IM region. Numerous vascular sinusoids and thin-walled vessels were observed. H&E-stained sections showed no evidence of inflammation in response to MCA, nor any evidence of infection. Histomorphometry of the two MCA-grafted sites examined showed that a mean of 71% of the bone tissue present in the defect site represented new bone formation, while 29% represented residual unresorbed MCA matrix. The residual MCA matrix occupied a mean of 13% of the total defect area.

TyrPC_{PL}/TCP demonstrated bone formation that was most extensive in the PC region and appeared to originate

TABLE 3. GROUP SEPARATION TABLE OBTAINED BY TUKEY-KRAMER METHOD ANALYSIS IN THE INTRAMEDULLARY CENTER DEFECT REGION

	Groups ^a			Mean (log)	Geometric mean (% BV)
MCA	A			-1.63	19.52
MCA + BMC	A			-1.73	17.96
TyrPC _{PL} /TCP		B		-4.50	1.11
PPF4 _{SLA} /HA _{PLGA} Dip		B	C	-4.65	0.96
PPF2 _{SLA} /HA _{PLGA} Dip		B	C	-4.72	0.89
TyrPC/TCP _{3DP}		B	C	-5.60	0.37
PLCL/TCP _{3DP}		B	C	-6.04	0.24
PLGA/TCP _{3DP}		B	C	-6.20	0.20
TyrPC _{PL}		B	C	-6.32	0.18
PLCL/TCP _{3DP} + BMC		B	C	-6.59	0.14
TyrPC _{PL} /CaCl ₂			C	-6.97	0.09
PLCL/TCP _{3DP}			D	-6.98	0.09
PPF2 _{SLA} /HA _{PLGA} Spray			D	-7.98	0.03
PPF2 _{SLA} /TCP _{PLGA} Spray			D	-8.05	0.03
TyrPC _{3DP}			D	-8.24	0.03
TyrPC _{3DP}			D	-8.62	0.02

^aScaffold formulations that are designated by the same letter group are statistically not different from each other, but are statistically different from scaffolds in nonoverlapping groups. The formulations labeled "A" had greater % bone volume than all other scaffolds.

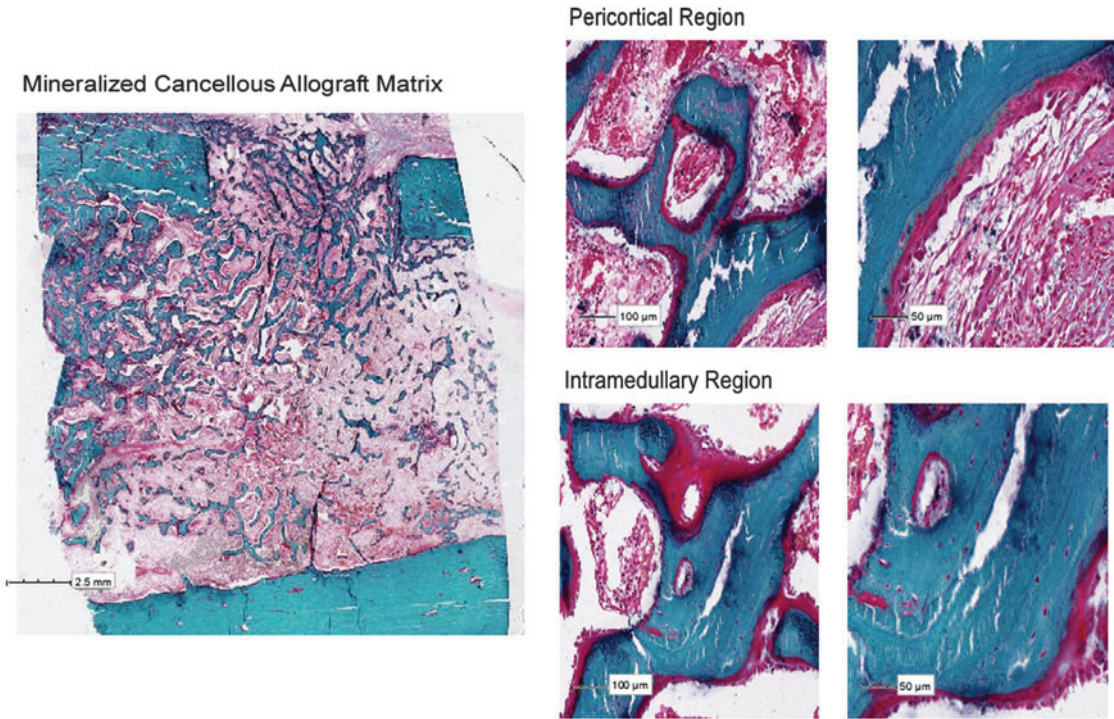


FIG. 8. Higher magnification of MCA samples stained with Goldner's Trichrome stain.

from the periosteal, cortical, and endosteal surfaces. Active bone formation was observed, with new mineralized bone containing a high density of osteocytes and cuboidal osteoblasts. Active osteoclasts eroded the bone surface. The scaffold had degraded substantially and was no longer identifiable as an organized structure. Residual scaffold material was found to occupy 31% of the defect area. Regions

of residual scaffold were frequently associated with a local fibrous tissue reaction without evidence of acute inflammation. Residual TCP may have added mineral density that slightly increased the overall % BV estimate, but was not considered to represent a major source of error.

The bone ingrowth in defects grafted with TyrPC_{PL}/CaCl₂ was distributed throughout the PC and IM regions. There

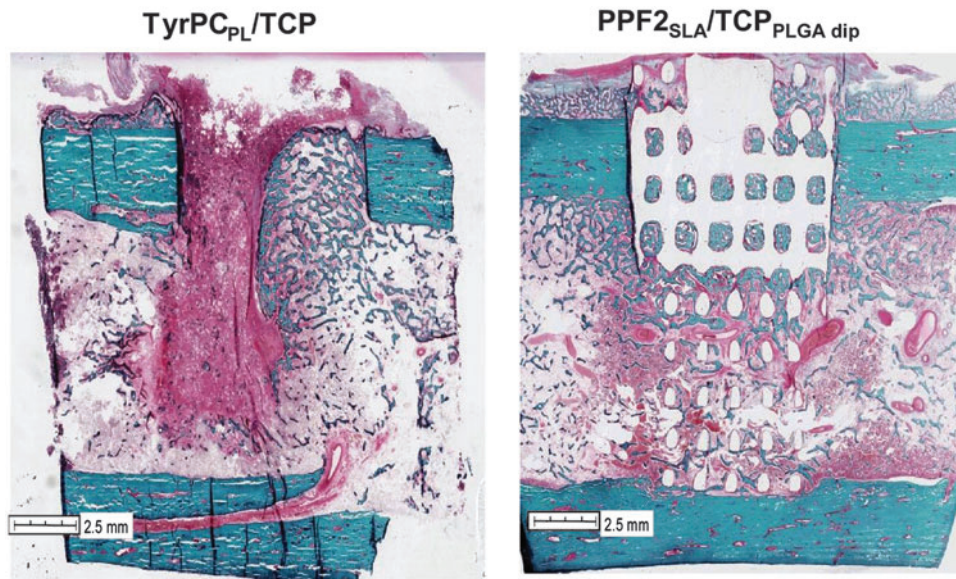


FIG. 9. Example of histology slides for TyrPCPL/TCP and PPF2SLA/TCPPLGA spray samples stained with Goldner's Trichrome stain revealing that trabecular bone formation is present and can penetrate deeply into the scaffold constructs in some areas. In the case of the PPF material, no significant resorption is seen and bone formation is most prominent in the pores of the scaffold within the PC region of the defect. In the case of the Tyr-PC scaffold, significant degradation of the scaffold is evident, and trabecular bone formation on the right side of the defect is seen penetrating into the deeper portion of the defect in some areas, while in other areas left side of the defect demonstrate a reactive fibrous tissue response.

was no evidence of residual local toxicity from the initial acid and hyperosmolar environment expected with CaCl_2 delivery. Again, residual polymer/scaffold was present in 31% of the defect area. New bone formation was evident with active secretory osteoblasts, osteoclastic resorption, and a high density of osteocytes in the new bone.

PPF₂_{SLA} scaffolds with TCP+PLGA or with HA+PLGA spray coatings showed that the PPF polymer scaffold remained intact as an organized structure at 4 weeks. Active bone formation was observed, with new mineralized bone containing a high density of osteocytes and cuboidal osteoblasts and active remodeling. Residual polymer occupied ~60% of the defect region. The histology suggested that the HA+PLGA surface coating had delaminated from the polymer surface and migrated into adjacent tissue within the defect. New bone formation occurred in the scaffold macropores, often on the surface of the PPF scaffold, and was most extensive in the PC defect region.

PLCL/TCP_{3DP} samples showed bone ingrowth at the edge of the defect area, predominantly from the cortical and endosteal surface. The PLCL/TCP_{3DP} scaffolds had degraded substantially and no longer had an organized structure. The area occupied by unresorbed polymer was ~36% of the defect.

Discussion

This work was undertaken with the goal of developing improved therapies for large segmental post-traumatic defects of bone by rapid assessment and comparison of several promising osteoconductive degradable polymer scaffolds. The performance of the polymeric scaffolds was compared to that of the current standard for osteoconductive materials (MCA), with the expectation of identifying one or more scaffold constructs that were worthy of further optimization in combination with sources of osteogenic cells and/or delivery of bioactive agents. These goals were met.

There are over 50 current products that are marketed for clinical use as bone void fillers. These products have received FDA clearance through the 510K mechanism based on their substantial equivalence to the performance of the predicate standard of MCA bone, which remains the most widely used osteoconductive bone graft material. The initial hope and expectation of this work was that one or more of the available formulations of polymer scaffolds would meet or exceed the performance of MCA. The data presented here demonstrate that the performance of the polymer scaffolds that have been tested thus far fall short of that expectation. MCA exceeded the performance of all polymer scaffolds, and remains the gold standard among osteoconductive bone scaffold materials for future comparisons.

While MCA remains the standard to beat, it must be pointed out that not all allograft materials are equal. The potential for variation in performance is one of the potential limitations of allograft as a therapeutic agent for bone regeneration. Different formulations and processing methods can change the biological performance of allograft. Even when the same processing methods are used, efficacy can vary between batches and/or donors. As a result, most providers of allograft bone, in addition to testing sterility, also perform biochemical and biological assays on the final allograft product to confirm consistency in potency and

performance. These tests may include biochemical assays to measure BMP-2 content, *in vitro* assay of the response of cells to allograft materials, or *in vivo* assays of biocompatibility and osteoinductivity.⁴¹⁻⁴⁶ Ongoing efforts to refine the formulation of allograft-derived scaffold materials through processing methods will continue to advance the reproducibility and efficacy of allograft scaffolds, customization of formulations for specific applications and their specialized use as delivery systems in combination with cells and bioactive materials. That said, the performance of allograft in these studies can be considered to be representative of the expected clinical performance of MCA allograft. The processing methods that were used are common standards in the industry. Two separate donors were used in grafting the 10 study subjects in Experiment 8. There was no difference in performance between bones derived from these two donors.

Despite the ongoing limitations of the polymer scaffold formulations tested here, the process of utilizing the CFMD model as a system for objective comparison of performance between scaffolds was a success. Significant differences were found between polymer scaffolds, and these observations can now be used to guide ongoing modifications and optimization of the design and use of polymer scaffold constructs. These data, in addition to prior experience,^{39,47} demonstrate that the CFMD model system is a robust and sensitive system with which to make objective comparisons between materials. The CFMD model allows these comparisons to be made in a rapid and efficient manner (only 4 weeks) using a large animal system, in a defect of clinically relevant size. By collecting four data points from each animal, the CFMD model maximizes the value of each subject and minimizes the number of subjects that are needed to provide sufficient power for comparisons. Moreover, in addition to total bone formation and histology, the CFMD model provides an opportunity in one model to assess the pattern, distribution, and remodeling features associated with a material in varying biological settings. The PC region models an environment in which sources of osteogenic cells are robust and can be derived from periosteum, cortex, or endosteum, while assessment in the IM region models an environment in which osteogenic cells are less abundant and the defect site is bounded by hematopoietic marrow and fat. These conditions are not as severe as the defect sites that are the target of treatment, but are clearly challenging enough to stratify the performance of available scaffold materials and detect significant differences in performance.

The value of the CFMD model as a tool for evaluation of bone grafting strategies is not limited to the evaluation of osteoconductive scaffold materials as presented here. The CFMD model has been shown to be an effective tool for comparison of cell sourcing and processing strategies,⁴⁸ and methods involving growth factor delivery use.³⁸ The CFMD model is currently being evaluated for use in assessment of methods to optimize the microenvironment for cell transplantation (e.g., the use of platelet gel preparations), and the selective surface modification of biomaterials (e.g., presentation of tethered growth factors).

The demonstrated utility of the CFMD model does not, however, displace the value of using smaller animal model systems in the rat (calvarial or femoral defect) or rabbit (calvarial or radius defect). In most biomaterial evaluations, it is most appropriate to prescreen materials for efficacy in

these smaller and less rigorous models before advancing scaffolds into more rigorous large animal models.

Despite the limitation in performance of the polymeric scaffolds in this study, ongoing work in the design and development of these and other scaffolds based on degradable synthetic or natural polymers is well justified. Synthetic polymer scaffolds have potentially large theoretical advantages over allograft scaffolds. Polymer scaffolds are almost certainly more reproducible than scaffolds made from allografts that are derived from highly standardized starting materials. In addition, several fabrication methods enable polymer scaffolds to be designed with highly controlled geometric features that might be customized for specific sites and applications. Polymer scaffolds also enable systematic and controlled modification of surface chemistry (e.g., tethered biomolecules), surface texture, drug delivery kinetics, and other features that are beyond the scope of control of current allograft processing methods.

Two scaffold constructs, TyrPC_{PL}/TCP and PPF_{4SLA}/HA_{PLGA} Dip, were found to be significantly better than alternative constructs, both when considering % BV measured in the overall region of the implant and when considering just the most biologically challenging center region of the IM region. While comparable in performance based on % BV measurements, these two scaffolds differ greatly in substrate material, structure, surface texture, surface chemistry, and degradation properties.

PPF_{4SLA}/HA_{PLGA} Dip represents a porous PPF scaffold that is manufactured using SLA and subsequently spray coated with PLGA and HA suspended in chloroform. This provides a highly regular and fully interconnected porous structure with pore size of 1000 microns and wall thickness of 500 microns. The walls of the PPF scaffolds are relatively smooth and are nonporous, providing a modest surface area on which a coating of HA nanoparticles and PLGA 50:50 was applied, and on which other bioactive agents or cells might be presented in the future. (Fig. 2) The PPF_{4SLA}/HA_{PLGA} Dip is, by design, a very slowly degrading polymer that has degraded little in the first 4 weeks following implantation in the CFMD model. This scaffold is also designed to have the capacity to serve as a structural load bearing or load-sharing construct in a bone defect site. This is a potentially valuable attribute in many clinical settings, particularly segmental bone defects. The mechanical properties of PPF scaffolds vary depending on resin composition and porosity, but typically exhibit a compressive strength ranging from 0.4 to 69 MPa, and a compressive modulus of 1.5 to 195 MPa.^{23,26,30}

In the current model, the capacity to bear load is not a particular advantage, nor is the limited amount of degradation, since any part of the defect site that is occupied by polymer is automatically unavailable for new bone formation. No accommodation or adjustment was made in the analysis that is presented here to consider just the % BV of bone formed within the available porous volume of the total volume of the PPF_{4SLA}/HA_{PLGA} Dip scaffolds in the 1 cm diameter × 1.5 cm length of the defect volume in the CFMD model. Were such an adjustment made, the relative volume of bone formed in these sites would be more than doubled for PPF_{4SLA}/HA_{PLGA} Dip and other PPF scaffolds. However, this would not significantly change the relative performance of PPF_{4SLA}/HA_{PLGA} Dip when compared to either TyrPC_{PL}/TCP or MCA.

The experiments evaluating PPF scaffolds that are described here allowed two comparisons to be made. In Experiment 4,

PPF substrates with a mean molecular weight of 2000 and 4000 were compared. The slower degrading PPF_{4SLA}/HA_{PLGA} Dip performed better based on mean % BV, but the difference was not statistically different. In Experiment 6, coatings containing HA + PLGA or TCP + PLGA were compared. There was no difference in performance and the variance was wider than in Experiment 4. Further improvement in the performance of PPF scaffolds is currently focusing on modification of the surface coating and/or the delivery of local bioactive agents or cells. For example, Kempen *et al.* have shown that PPF scaffolds can be used to deliver BMP-2 or VEGF.²⁴

The evaluations performed with TyrPC-based scaffolds in these studies have identified parameters that are under ongoing optimization. In Experiment 2, a benefit was found when calcium mineral was added to a TyPC scaffold fabricated using 3DP. In Experiment 3, a benefit was found in moving from a 3DP fabrication strategy to a PL method. The increase in bone formation that was seen is possibly due to the highly interconnected, bimodal pore structure and higher overall porosity that results from the PL fabrication process.¹² In Experiment 7, the benefit of adding calcium mineral to PL scaffolds was confirmed, using either β -TCP or the highly soluble CaCl₂. β -TCP performed better, however, perhaps due to prolonged residence within the scaffold. Despite the relatively rapid degradation that was designed for this polymer, histological assessment suggested that ~30% of the defect site was still occupied by polymeric materials after 4 weeks *in vivo*, and that fibrous tissue formation was common in regions where fragments of the bulk polymer were retained. Further modification of structural or degradation properties, or the composition of calcium containing agents, may improve the reliability of bone formation.

Finally, in addition to demonstrating that the CFMD model has substantial value in the assessment of scaffolds and surface coatings in general, and in determining whether further changes in the current scaffolds may result in significant improvement in performance in particular, these data also point to a possible ceiling effect limitation in this model with respect to performance measurement based on mineralization alone as an estimate of new bone formation. Specifically, the performance that has been documented for MCA is likely at or close to the upper limit of performance that might be expected from any osteoconductive material in this model when mineralization and MicroCT alone are used as the outcome parameter. As a result, the CFMD model may be insensitive to the detection of further improvements in performance that might be achieved by combination of MCA with cell therapy approaches or the delivery of bioactive agents unless MicroCT data are combined with histology and histomorphometry, which would allow quantitative assessment of remodeling as well as bone formation as an outcome metric. As a result, in order to further advance the performance of MCA or other allograft constructs combined with other cell sourcing options or bioactive agents using the CFMD model, histomorphometry will be added as an intrinsic outcome metric. Consideration can also be made for advancement of high-performing materials into more stringent models, such as the chronic caprine tibial defect model that has been recently reported.³⁷

Conclusion

MCA remains the current standard for osteoconductive scaffolds. The polymer scaffold constructs tested thus far in

the CFMD model, while conceptually promising, do not approach the level of performance that is achieved by MCA. Ongoing work on polymer scaffolds is still justified, however. The potential for surface modification using variations of calcium-containing surface coatings and/or the delivery of BMP-2 to improve the performance of these scaffold constructs is currently being tested.

The work in this article further establishes the CFMD model as a platform of testing methodology and performance metrics that can now be used to measure the relative efficacy of many scaffold materials and surface coatings. This platform of experience and data further enables the subsequent assessment of the added benefit of cell therapy approaches and bioactive agents (e.g., BMPs) on these or other bulk scaffold materials.

Ongoing work to further optimize the use of MCA in severe segmental defects will evaluate MCA as a delivery vehicle for osteogenic cell sources and/or in combination with bioactive adjuvant materials. Future studies will utilize the CFMD model, but ultimately require the use of the more stringent models, such as the chronic caprine tibial defect model that was described above.³⁷

Acknowledgments

This work was funded by the Armed Forces Institute of Regenerative Medicine (AFIRM), which is managed and funded through the U.S. Army Medical Research and Materiel Command (MRMC). The AFIRM has additional funding from the U.S. Navy, the Office of Naval Research, the U.S. Air Force Office of the Surgeon General, the National Institutes of Health, the Veterans Administration, the Cleveland Clinic, and local public and private matching funds. This publication was supported by a subcontract from Rutgers University, Department of Chemistry and Chemical Biology/NJ Center for Biomaterials, under Cooperative Agreement No. WSIXWH-08-2-0034 from the U.S. Department of Defense I U.S. Army Medical Research Acquisition. This work was also supported by the Musculoskeletal Transplant Foundation (Edison, NJ).

We acknowledge Dr. Joachim Kohn and Dr. Aniq Darr for preparation and characterization of TyrPC scaffolds and for contributions in editing the manuscript. We also gratefully acknowledge Jason Bryan, Cynthia Boehm, Tess Henderson, Brandon Lampe, Carynne Fox, Richard Rozic, Thomas Patterson, James Herrick, Julie Burgess, Glenda Evans, and Suzanne Segovis for their technical assistance.

Disclosure Statement

Viviane Luangphakdy, M.S.—No conflicts.

Esteban Walker, Ph.D.—No conflicts.

Kentaro Shinohara, M.D., Ph.D.—No conflicts.

Hui Pan, M.D., Ph.D.—No conflicts.

Theresa Hefferan, Ph.D.—No conflicts.

Thomas Bauer, M.D., Ph.D.—Consultant for Stryker Orthopaedics. Deputy Editor for Research for the Journal of Bone and Joint Surgery.

Linda Stockdale, M.A.T.—No conflicts.

Sunil Saini, Ph.D.—Employee of Integra Life Sciences.

Mahrokh Dadsetan, Ph.D.—No conflicts.

M. Brett Runge, Ph.D.—No conflicts.

Amit Vasanji, Ph.D.—No conflicts.

Linda Griffith, Ph.D.—Potential for royalties related to 3D Printing technology licensed from MIT.

Michael Yaszemski, M.D., Ph.D.—Founder, with equity in BonWrx, which has licensed PPF technology. Deputy Editor for *Journal for Biomedical Materials Research Part A*. Publisher J. Wiley.

George F. Muschler, M.D.—No conflicts.

Two collaborators in this work have elected not to be credited as co-authors, but contributed significantly to this work by providing materials for testing and providing editing and review of the manuscript. Their conflicts are listed below, in the event that the editors of *Tissue Engineering* feel that these should be cited with the published article:

Aniq Darr, Ph.D. (Rutgers University)—Consultant for Trident Biomedical.

Joachim Kohn, Ph.D. (Rutgers University)—Stockholder and founder of Trident Biomedical.

References

- Owens, B.D., *et al.* Characterization of extremity wounds in operation Iraqi freedom and operation enduring freedom. *J Orthop Trauma* **21**, 254, 2007.
- Muschler, G.F., Nakamoto, C., and Griffith, L.G. Engineering principles of clinical cell-based tissue engineering. *J Bone Joint Surg Am* **86-A**, 1541, 2004.
- Griffith, L.G. Emerging design principles in biomaterials and scaffolds for tissue engineering. *Ann NY Acad Sci* **961**, 83, 2002.
- Griffith, L.G., and Naughton, G.K. Tissue engineering—current challenges and expanding opportunities. *Science* **295**, 1009, 2002.
- Hubbell, J.A. Bioactive biomaterials. *Curr Opin Biotech* **10**, 123, 1999.
- Muschler, G.F., and Lane, J.M. Spine fusion: principles of bone fusion. In: Herkowitz, H.N., *et al.*, eds. *The Spine*. Philadelphia: WB Saunders, 1999, pp. 1573–1589.
- Bauer, T.W., and Muschler, G.F. Bone graft materials. An overview of the basic science. *Clin Orthop* **371**, 10, 2000.
- Siemionow, K.B., and Muschler, G.F. Principles of bone fusion. In: Herkowitz, H.N., *et al.*, eds. *Rothman-Simeone The Spine*. Philadelphia, PA: Saunders, 2011, pp. 1130–1158.
- Bourke, S.L., and Kohn, J. Polymers derived from the amino acid L-tyrosine: polycarbonates, polyarylates and copolymers with poly(ethylene glycol). *Adv Drug Deliv Rev* **55**, 447, 2003.
- Hooper, K.A., Macon, N.D., and Kohn, J. Comparative histological evaluation of new tyrosine-derived polymers and poly (L-lactic acid) as a function of polymer degradation. *J Biomed Mater Res* **41**, 443, 1998.
- James, K., *et al.* Small changes in polymer chemistry have a large effect on the bone-implant interface: evaluation of a series of degradable tyrosine-derived polycarbonates in bone defects. *Biomaterials* **20**, 2203, 1999.
- Magno, M., *et al.* Synthesis, degradation and biocompatibility of tyrosine-derived polycarbonate scaffolds. *J Mater Chem* **20**, 8885, 2010.
- Lee, K.W., *et al.* Poly(propylene fumarate) bone tissue engineering scaffold fabrication using stereolithography: effects of resin formulations and laser parameters. *Biomacromolecules* **8**, 1077, 2007.
- Lee, K.W., *et al.* Fabrication and characterization of poly(propylene fumarate) scaffolds with controlled pore structures using 3-dimensional printing and injection molding. *Tissue Eng* **12**, 2801, 2006.
- Zhu, X., *et al.* Effects of composite formulation on the mechanical properties of biodegradable poly(propylene

- fumarate)/bone fiber scaffolds. *Int J Polym Sci* **2010**, pii: 270273, 2010.
16. Griffith, L.G., and Grodzinsky, A.J. Advances in biomedical engineering. *JAMA* **285**, 556, 2001.
 17. Hammouche, S., Hammouche, D., and McNicholas, M. Biodegradable bone regeneration synthetic scaffolds in tissue engineering. *Curr Stem Cell Res Ther* **7**, 134, 2012.
 18. Solchaga, L.A., *et al.* Repair of osteochondral defects with hyaluronan- and polyester-based scaffolds. *Osteoarthritis Cartilage* **13**, 297, 2005.
 19. Roy, T.D., *et al.* Performance of degradable composite bone repair products made via three-dimensional fabrication techniques. *J Biomed Mater Res A* **66**, 283, 2003.
 20. Roy, T.D., *et al.* Performance of hydroxyapatite bone repair scaffolds created via three-dimensional fabrication techniques. *J Biomed Mater Res A* **67A**, 1228, 2003.
 21. Saini, S., Muschler, G.F., and McGlohorn, J. The effect of bone graft architecture on bone formation in a canine defect model. Chicago, IL: Orthopedic Research Society, 2006.
 22. Abbah, S.A., *et al.* Biological performance of a polycaprolactone-based scaffold used as fusion cage device in a large animal model of spinal reconstructive surgery. *Biomaterials* **30**, 5086, 2009.
 23. Fisher, J.P., Dean, D., and Mikos, A.G. Photocrosslinking characteristics and mechanical properties of diethyl fumarate/poly(propylene fumarate) biomaterials. *Biomaterials* **23**, 4333, 2002.
 24. Kempen, D.H., *et al.* Effect of local sequential VEGF and BMP-2 delivery on ectopic and orthotopic bone regeneration. *Biomaterials* **30**, 2816, 2009.
 25. Lee, K.W., *et al.* Enhanced cell ingrowth and proliferation through three-dimensional nanocomposite scaffolds with controlled pore structures. *Biomacromolecules* **11**, 682, 2010.
 26. Rajagopalan, S., and Robb, R.A. Schwarz meets Schwann: design and fabrication of biomorphic and durataxic tissue engineering scaffolds. *Med Image Anal* **10**, 693, 2006.
 27. Sawyer, A.A., *et al.* The stimulation of healing within a rat calvarial defect by mPCL-TCP/collagen scaffolds loaded with rhBMP-2. *Biomaterials* **30**, 2479, 2009.
 28. Sherwood, J.K., *et al.* A three-dimensional osteochondral composite scaffold for articular cartilage repair. *Biomaterials* **23**, 4739, 2002.
 29. Eid, K., *et al.* Effect of RGD coating on osteocompatibility of PLGA-polymer disks in a rat tibial wound. *J Biomed Mater Res* **57**, 224, 2001.
 30. Wang, S., Lu, L., and Yaszemski, M.J. Bone-tissue-engineering material poly(propylene fumarate): correlation between molecular weight, chain dimensions, and physical properties. *Biomacromolecules* **7**, 1976, 2006.
 31. Kempen, D.H., *et al.* Effect of autologous bone marrow stromal cell seeding and bone morphogenetic protein-2 delivery on ectopic bone formation in a microsphere/poly(propylene fumarate) composite. *Tissue Eng Part A* **15**, 587, 2009.
 32. Kempen, D.H., *et al.* Retention of *in vitro* and *in vivo* BMP-2 bioactivities in sustained delivery vehicles for bone tissue engineering. *Biomaterials* **29**, 3245, 2008.
 33. Kim, C.W., *et al.* Characterization of porous injectable poly(propylene fumarate)-based bone graft substitute. *J Biomed Mater Res A* **85**, 1114, 2008.
 34. Zeltinger, J., *et al.* Effect of pore size and void fraction on cellular adhesion, proliferation, and matrix deposition. *Tissue Eng* **7**, 557, 2001.
 35. Cooke, M.N., *et al.* Use of stereolithography to manufacture critical-sized 3D biodegradable scaffolds for bone ingrowth. *J Biomed Mater Res* **64B**, 65, 2003.
 36. Garber, J.C., *et al.* Guide for the Care and Use of Laboratory Animals. Committee for the Update of the Guide for the Care and Use of Laboratory Animals, Institute for Laboratory Animal Research, Division of Earth and Life Studies, National Research Council of the National Academies: Washington, D.C. 2011.
 37. Muschler, G., *et al.* The design and use of animal models for translational research in bone tissue engineering and regenerative medicine. *Tissue Eng Part B Rev* **16**, 123, 2010.
 38. Takigami, H., *et al.* Bone formation following OP-1 implantation is improved by addition of autogenous bone marrow cells in a canine femur defect model. *J Orthop Res* **25**, 1333, 2007.
 39. Muschler, G.F., Boehm, C., and Easley, K. Aspiration to obtain osteoblast progenitor cells from human bone marrow: the influence of aspiration volume. *J Bone Joint Surg Am* **79**, 1699, 1997.
 40. Muschler, G.F., *et al.* Spine fusion using cell matrix composites enriched in bone marrow-derived cells. *Clin Orthop Rel Res* **407**, 102, 2003.
 41. Bae, H., *et al.* Variability across ten production lots of a single demineralized bone matrix product. *J Bone Joint Surg Am* **92**, 427, 2010.
 42. Bae, H.W., *et al.* Intervariability and intravariability of bone morphogenetic proteins in commercially available demineralized bone matrix products. *Spine (Phila Pa 1976)* **31**, 1299; discussion 1307, 2006.
 43. Sun, P., Han, J., and Weng, Y. The antidotal effects of high-dosage gamma-aminobutyric acid on acute tetramine poisoning as compared with sodium dimercaptopropane sulfonate. *J Huazhong Univ Sci Technolog Med Sci* **27**, 419, 2007.
 44. Han, B., Tang, B., and Nimmi, M.E. Quantitative and sensitive *in vitro* assay for osteoinductive activity of demineralized bone matrix. *J Orthop Res* **21**, 648, 2003.
 45. Dunn, M., *et al.* Effect of allograft processing on structural cortical grafts: a comparison of three proprietary processing methods. In: Proceedings of NASS 23rd Annual Meeting, Toronto, Ontario, Canada, Oct 14–18, 2008. *The Spine Journal* **8**, 78, 2008.
 46. Jurgensmeier, D., and Hart, R. Variability in tissue bank practices regarding donor and tissue screening of structural allograft bone. *Spine (Phila Pa 1976)* **35**, E702, 2010.
 47. Muschler, G.F., *et al.* Selective retention of bone marrow-derived cells to enhance spinal fusion. *Clin Orthop* **242**, 2005.
 48. Caralla, T., Joshi, P., Boehm, C., Hefferan, T., Herrick, J., Luangphakdy, V., Fleury, S., Yaszemski, M., Zborowski, M., and Muschler, G. Concentration and Selection of Osteogenic Progenitors using Magnetic Labeling based on Hyaluronan Expression for Immediate Transplantation into a Canine Femoral Multidefect Model. In: TERMIS Annual Meeting, Houston, TX. December 11–14, 2011.

Address correspondence to:

George F. Muschler, MD
 Department of Biomedical Engineering (ND20)
 Lerner Research Institute
 Cleveland Clinic
 9500 Euclid Ave.
 Cleveland, OH 44195

E-mail: muschlg@ccf.org

Received: May 8, 2012

Accepted: September 25, 2012

Online Publication Date: January 21, 2013